Available online at www.sciencedirect.com

SciVerse ScienceDirect

Journal of the European Ceramic Society 32 (2012) 1983–1987

www.elsevier.com/locate/jeurceramsoc

Nanocrystaline solid solution CeO_2–Bi_2O_3

M. Prekajski [a,*], Z. Dohčević-Mitrović [b], M. Radović [b], B. Babić [a], J. Pantić [a], A. Kremenović [c], B. Matović [a]

[a] *Institute of Nuclear sciences Vinca, PO Box 522, 11001 Belgrade, Serbia*
[b] *Institute of Physics, Pregrevica 118, 11080 Belgrade, Serbia*
[c] *Faculty of Mining and Geology, University of Belgrade, Đušina 7, 11000 Belgrade, Serbia*

Available online 21 January 2012

Abstract

Nanocrystalline powders of solid solution CeO_2–Bi_2O_3 were synthesized by self-propagating room temperature reaction (SPRT) procedure with composition $(Ce_{1-x}Bi_xO_{2-\delta}$ where the $x = 0.1$–0.5). X-ray diffraction analyses show that for $x < 0.50$ a solid solution with fluorite structure is formed. Rietveld's structure refinement method was applied to characterize prepared powders and its microstructure (size–strain). The lattice parameters increase according to Vegard's rule with increasing of Bi concentration. The average crystallite size is about 2–3 nm. Spectroscopic ellipsometry and Raman scattering measurements were used to characterize the samples at room temperature. The Raman measurements demonstrated electron molecular vibrational coupling and increase of oxygen vacancy concentration whereas increase of Bi content provokes a small decrease of optical absorption edge in comparison with pure ceria. Specific surface area of obtained powders was measured by Brunauer–Emmet–Teller (BET) method.

Keywords: Self-propagating reaction; CeO_2; Bi_2O_3; X-ray methods; Spectroscopy

1. Introduction

Oxide solid solutions $(CeO_2)_{1-x}(BiO_{1.5})_x$ are expected to be a novel electrolyte exhibiting new electrochemical transport properties because ceria-based solid solutions doped with lower valence ions usually possess oxide ion conductivity higher than yttrium-stabilized zirconia (YSZ) and because the oxide ionic conductivity of δ-Bi_2O_3 is the highest to date. Both δ-Bi_2O_3 and CeO_2 have fluorite type of structure, but there are some structural misfits because of the differences in ionic radius size and valence state ($r(Bi^{3+}) = 0.117$ nm and $r(Ce^{4+}) = 0.097$ nm[1]). Anyway structural similarity between these oxides favors a high solubility of Bi in CeO_2 by enlarging the cell volume and retaining cubic symmetry.[2]

Various methods of synthesis have been used in order to obtain CeO_2–Bi_2O_3 solid solution, such as high temperature ceramic method,[3] low temperature hydrothermal synthesis,[4] PVA polymerization process,[5] combustion process in combination with hydrothermal analysis[6] and coprecipitation route.[7] It was found that the solubility of Bi in structure of CeO_2 is <50%.[2] But still one of the major problem is that all of this methods for synthesis involves multiple steps of mixing, grinding and firing on high temperatures, so it would be of great interested to synthesize this material by simple method on lower temperatures with the preference of forming nanocrystalline solids. One of the methods that is cost and time effective is the self propagating room temperature (SPRT) synthesis (with whom we were able to produce nanocrystalline materials with an average crystallite size below 10 nm). This method was already successfully used for synthesis of other CeO_2 based nanopowders[8–10] and α-Bi_2O_3.[11]

The aim of this work was to use this simple and effective SPRT method in order to obtain obtained nanosized powder sample of CeO_2–Bi_2O_3 solid solution, with crystallite size less than 5 nm.

2. Experimental

2.1. Synthesis procedure

Nanocrystalline CeO_2–Bi_2O_3 was synthesized by a SPRT method using cerium nitrate hexahydrate (Riedel-de Haën, 99%

* Corresponding author. Tel.: +381 11 3408224; fax: +381 11 3408224.
E-mail address: prekajski@vinca.rs (M. Prekajski).

0955-2219/$ – see front matter © 2011 Elsevier Ltd. All rights reserved.
doi:10.1016/j.jeurceramsoc.2011.12.009

purity), bismuth nitrate pentahydrate (Riedel-de Haën, 99% purity) and sodium hydroxide (Lach-Ner, 99% purity) as starting materials. Preparation of $Ce_{1-x}Bi_xO_{2-\delta}$ powder was performed according to reaction:

$$(1-x)Ce(NO_3)_3{\cdot}6H_2O + xBi(NO_3)_3{\cdot}5H_2O + 3NaOH + (½-\delta)O_2 \rightarrow Ce_{1-x}Bi_xO_{2-\delta} + 3NaNO_3 + yH_2O \quad (1)$$

The above reaction proceeds at room temperature after the mixture of reactants was mechanically activated by hand mixing in alumina mortar for 5–7 min, until the mixture gets light yellow. After being exposed to air for 3 h, the mixture was suspended in water in order to eliminate $NaNO_3$. Rinsing was performed in centrifuge — Centurion 1020D, at 3500 rpm for 10 min. This procedure was performed four times with distilled water and twice with ethanol, and after that, material was dried out at 60 °C in ambient atmosphere.

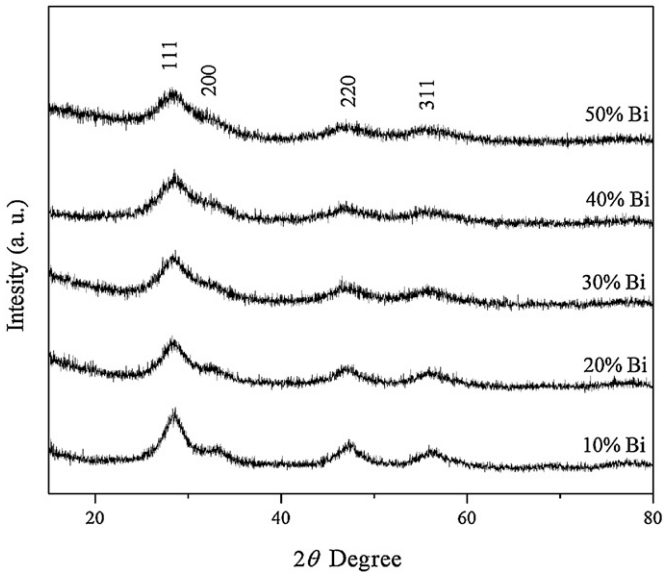

Fig. 1. X-ray diffraction patterns of $Ce_{1-x}Bi_xO_{2-\delta}$ powders ($x = 0.1$, 0.2, 0.3, 0.4 and 0.5).

2.2. Characterization of synthesized nanopowders

The structure of obtained powder was determinate by X-ray powder diffraction on a Siemens D-500 XRPD diffractometer with Cu $K\alpha_{1,2}$ radiations, at room temperature. Data for structural refinement were taken in the 2θ range 20–70°, with the step of 0.03° and scanning time of 10 s per step. The refinement was performed with the FullProf computer program[12–14] which adopts the Rietveld calculation method. The TCH pseudo-Voigt profile function was used. To take instrumental broadening into account, the XRD pattern of a standard specimen CeO_2 was fitted by the convolution of the experimental TCH pseudo-Voigt function.[15]

Unpolarized Micro-Raman scattering measurements were performed in the backscattering configuration using Jobin Yvon T64000 spectrometer equipped with nitrogen cooled Symphony® charge-coupled-device detector (CCD). As an excitation source we used 514.5-nm line of Ar^+/Kr^+-ion laser operating at low power in order to avoid sample heating.

Ellipsometric measurements were performed in the UV–vis spectral range, using high resolution variable angle spectroscopic ellipsometer (SOPRA GES5E – IRSE) of the rotating polarizer type.

Adsorption and desorption isotherms of N_2 were measured on samples, at −196 °C, using the gravimetric McBain method. The specific surface area, S_{BET}, pore size distribution, mesopore including external surface area, S_{meso}, and micropore volume, V_{mic}, for the samples were calculated from the isotherms. Pore size distribution was estimated by applying BJH method[16] to the desorption branch of isotherms and mesopore surface and micropore volume were estimated using the high resolution α_s plot method.[17–19] Micropore surface, S_{mic}, was calculated by subtracting S_{meso} from S_{BET}.

3. Results and discussion

3.1. XRPD

The X-ray patterns show that synthesized powders are single phase solid solutions even for a very high concentration of Bi ions (Fig. 1). One can see that all patterns exclusively show diffraction peaks corresponding to CeO_2 fluorite structure indicating that that the Bi^{3+} ions are incorporated in ceria lattice instead of Ce^{4+} ions. None of the samples showed any evidence for impurity phases. This high solubility may be attributed to nonequilibrium condition, which is characteristic of nanometric powders. All peaks for each sample are significantly broadened indicating small crystallite size and/or strain. Also some reflections for corresponding atomic planes (hkl: 200, 400, 311, 420) are impossible to indicate due to low crystallinity of obtained powders.

Data reported by Kuemmerle and Heger[20] was used as starting structural model for Rietveld refinement. Refined structure and microstructure parameters are given in Table 1. Corresponding agreement factors are also given in Table 1. Reasonable values of R factors and χ^2 are an indication of good refinement. The lattice parameters (Table 1) of the identified fluorite structures in the X-ray patterns verified formation of ceria solid solutions according to which the lattice parameters increase according to the Vegard's rule with increasing of Bi^{3+} concentration. According to Shannon's compilation,[1] the ionic radii of Ce^{4+} and Bi^{3+} for CN 8, are 0.97 and 1.17 Å, respectively. Thus, mixing of Ce^{4+} and Bi^{3+} ions and increasing Bi^{3+} concentration will keep on enlarging cell lattice.

Values of averaged apparent crystallite size obtained by the refinement of the TCH-pV parameters for all samples are less than 4 nm. The values of microstrain increase with increasing of dopant concentration due to distorsion in CeO_2 crystal lattice

Table 1
Refined structural and microstructural parameters for $Ce_{1-x}Bi_xO_{2-\delta}$ samples ($x = 0.1$, 0.2, 0.3, 0.4 and 0.5) and corresponding agreement factors.

Sample	a (Å)	Crystallite size (nm)	Strain (10^3 Å)	R_p (%)	χ^2
$Ce_{0.9}Bi_{0.1}O_{2-\delta}$	5.4370(2)	3.60(1)	172	6.10	1.02
$Ce_{0.8}Bi_{0.2}O_{2-\delta}$	5.4470(1)	3.90(6)	214	9.76	1.07
$Ce_{0.7}Bi_{0.3}O_{2-\delta}$	54575(1)	3.92(3)	289	7.66	1.07
$Ce_{0.6}Bi_{0.4}O_{2-\delta}$	5.4640(2)	2.58(1)	350	7.12	1.00
$Ce_{0.5}Bi_{0.5}O_{2-\delta}$	5.4920(2)	3.41(5)	385	9.72	1.24

provoked by incorporation of larger Bi^{3+} ion on Ce^{4+} site in fluorite crystal lattice.

Recently, Hong proposed an equation for calculating lattice parameters of a fluorite structure based on the ion-packing model[21] described by following equation:

$$a = \left\{ \frac{4}{\sqrt{3}} \cdot [r_M - r_{Ce} - 0.25r_O + 0.25v_O] \cdot u + \frac{4}{\sqrt{3}} \cdot [r_{Ce} + r_O] \right\} \cdot 0.9971. \quad (2)$$

where r_M, r_{Ce}, r_O and r_{v_o} are the ionic radii of the dopant cation, cerium ion, oxygen ion and oxygen vacancy in Å, respectively; u is the dopant molar fraction.

Calculated according to Eq. (2), and measured lattice parameter a of doped ceria (Fig. 2) versus Bi^{3+} content, obeys Vegard's rule. The results show that there is very good agreement between experimental and calculated values. A small discrepancy can be attributed to changes in the anion vacancy radius or to decrease in the cation coordination number.[22] Since in dilute solution, the radius of a cation changes linearly with dopant concentration, then the anion radius must exhibit linear dependence with the increasing concentration of anion vacancies.[23] In this paper we used a fixed value of the oxygen vacancy radius (1.164 Å).[24] It is known that fixed value for anion vacancy radius is not accurate[23] and this might be responsible for observed small deviation. Also, some of the Ce^{4+} ions could be reduced to Ce^{3+} ions. Then Ce_2O_3 can be considered as a dopant in CeO_2 lattice. For small concentrations of Ce_2O_3, Vegard's rule is valid, thus the unit cell parameter of CeO_2 should be linearly dependent on the quantity of dopant (i.e. present Ce_2O_3).[25] It should be taken into account that additional presence of Ce^{3+} introduces new oxygen vacancies in the structure.

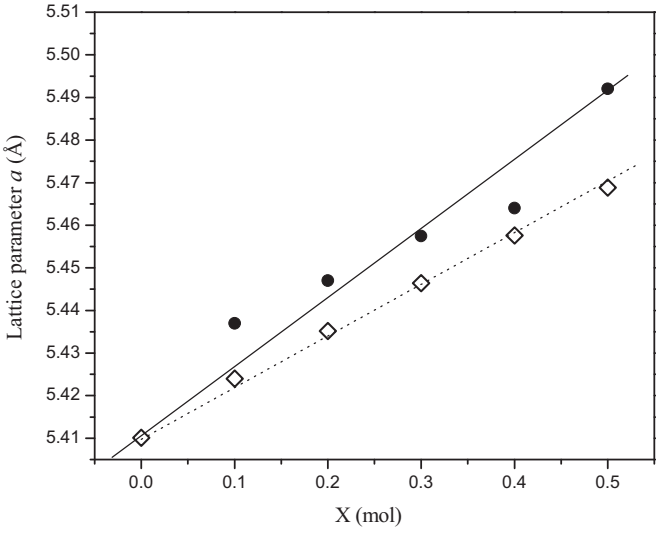

Fig. 2. Calculated (□) and measured (●) lattice parameter (a_o) of doped ceria as a function of Bi content in samples ($Ce_{1-x}Bi_xO_{2-\delta}$).

3.2. Raman spectral studies

Raman spectra of $Ce_{1-x}Bi_xO_{2-\delta}$ samples are presented in Fig. 3. For the low Bi concentrations ($x = 0.1$) three modes at 456, 520 and 600 cm^{-1} are presented. The Raman mode at ~456 cm^{-1} is assigned to the F_{2g} mode of CeO_2 fluorite structure.[26] The F_{2g} mode, in $Ce_{1-x}Bi_xO_{2-\delta}$ samples, shifts to lower frequencies and significantly broadens with increasing of dopant concentration up to 40%. This mode presents symmetrical stretching vibrations of CeO_8 vibration unit and should be very sensitive to the oxygen sublattice disorder and change of local environment with doping.[26] Additional modes, located at 529 cm^{-1} and 600 cm^{-1}, can be ascribed to presence of Bi^{3+} ions[27] and extrinsic and intrinsic oxygen vacancies generated as charge compensating defects induced by the incorporation of Bi^{3+} cations in ceria lattice.[28] Intensity of both oxygen vacancy modes increases with doping content up to 40%. For 50% Bi-doped samples these two modes merge almost in

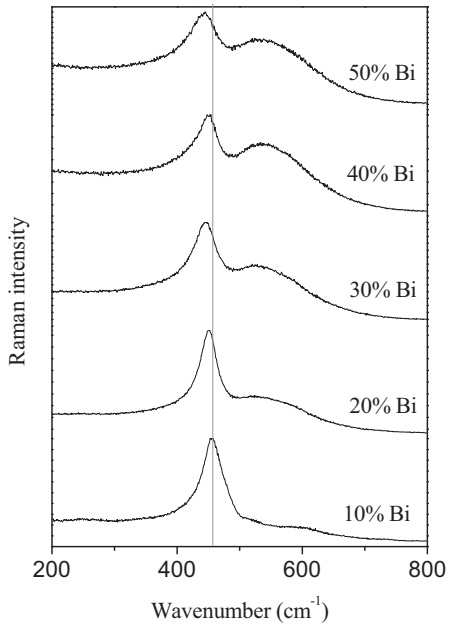

Fig. 3. Raman spectra of bismuth ceriom oxide solid solution.

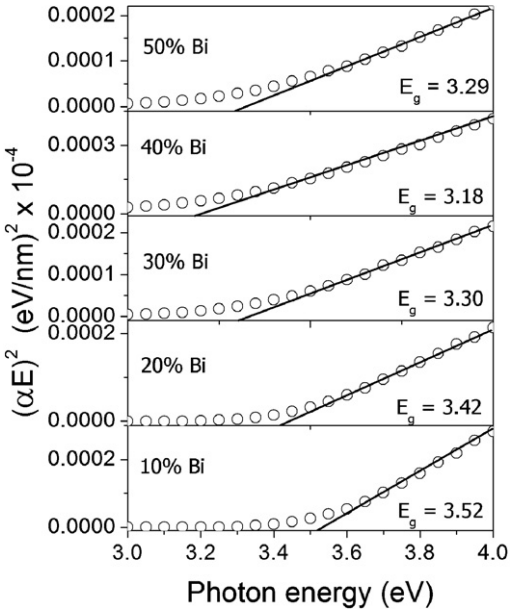

Fig. 4. $(\alpha E)^2$ versus photon energy plots for determination of band gap.

one very intensive mode followed by a drastic intensity decrease and minor blue shift of ceria F_{2g} mode. Observed shift of F_{2g} mode in this sample can be explained by Raman mode mixing with different optical phonon states due to high disorder and the presence of high defect concentration.[29]

From Raman scattering results it was confirmed the results obtained with X-ray powder diffraction that all synthesized powders are single phase solid solutions (with CeO_2 fluorite type of structure), which are independent of dopant concentration in the investigated range, with complex local atomic arrangement around Ce^{4+} and Bi^{3+} ions for high dopant concentration, which is on the other side very different from low doping regime (less than 40% of Bi).

3.3. Elipsometric measurements

The direct optical band gap (E_g) was evaluated from the general equation[15]:

$$(\alpha E)^2 = b(E - E_g) \quad (3)$$

where α is the absorption coefficient related to the measured extinction coefficient k ($\alpha = 4\pi k/\lambda$), E is photon energy and parameter b is related to the density of states in the conduction band. Linear plots of $(\alpha E)^2$ towards zero energy are shown in Fig. 4 and the values of band gap for Bi doped ceria samples were determined from these plots.

By analyzing the absorption behavior we can observe that doping with up to 40% of Bi^{3+} ions provokes a small decrease of band gap value – E_g, due to additional electronic levels introduced within the band gap. These states are originating from oxygen vacancy defect states[30] and electronic states of Bi^{3+} ions.

Further doping with Bi^{3+} ions lead to increase of band gap value. We assumed that the additional Bi^{3+} ions lead to increasing of the number of oxygen vacancies till certain dopant concentration following formation clusters of oxygen vacancies.[31] That also can explain the results obtained by Raman spectral studies, which show that samples with high concentration have different local atomic arrangement.

Table 2
Porous properties of Bi doped CeO_2 samples.

Sample	S_{BET} (m^2/g)	S_{meso} (m^2/g)	S_{mic} (m^2/g)	V_{mic} (cm^3/g)
10% Bi	45	20	25	0.016
20% Bi	39	12	27	0.016
30% Bi	84	39	45	0.027
40% Bi	209	89	120	0.071
50% Bi	20	11	9	0.006

3.4. Brunauer–Emmet–Teller (BET)

Specific surface areas calculated by BET equation, S_{BET}, are listed in Table 2. S_{BET} values, for all samples, lie within 20–209 m^2/g. Values of S_{BET} from Table 2 show that overall specific surface S_{BET} depends on the amount of doped Bi. The largest specific surface was detected at sample with 40% of Bi.

These results are in good agreement with results obtained by elipsometric measurements and Raman spectroscopy. They confirmed assumption that in samples with more than 40% of Bi oxygen vacancies starts to form clusters, which on the other hand have a significant impact on the physical properties of materials.

Pore size distribution (PSD) of samples shows that samples are mesoporous and microporous with most of the pores radius between 1.5 and 6 nm. Calculated porosity parameters (S_{meso}, S_{mic}, V_{mic}) are given in Table 2.

4. Conclusion

Solid solution between CeO_2 and Bi_2O_3 was successfully synthesized in range from 10 to 50% of Bi using simple, time and cost effective SPRT method of synthesis. It was found that the ceria powders with up to 50% of Bi are solid solution with fluorite type of crystal structure. All synthesized powders have particle size in nanometric range (less than 4 nm). The calculated and measured lattice parameters were compared and were found to be in a good agreement. Raman spectral studies confirmed that all synthesized powders are solid solution. Optical properties of CeO_2 nanoparticles are strongly correlated to synthesis parameters and doping with Bi ions provokes a small decrease of optical absorption edge. Monitoring and controlling the shift of optical band gap in ceria based nanomaterials can have significant implications in the field of photocatalysis and smart windows technologies. Specific surface area was measured and shows that the highest value for specific surface was detected at sample with 40% of Bi. Increased number of oxygen vacancies caused by doping with lower charge ion (Bi^{3+}) lead to the improvement of the characteristics of the synthesized samples (lower band gap and larger specific surface area). But on the other hand excessive concentration of oxygen vacancies leads to the formation of clusters which in this case bring the deterioration of the same optical properties.

Acknowledgment

This project was financially supported by the Ministry of Education and Science of the Republic of Serbia (Project number: 45012).

References

1. Shannon A. Revised effective ionic radii and systematic studies of interatomic distances in halides and chalcogenides. *Acta Crystallogr A* 1976;**32**:751–67.
2. Li Guangshe, li Liping, Feng Shouhua, wang Minqiang, Zhang Liangying, Yao Xi. An effective synthetic route for a novel electrolyte: nanocristalline Solid solutions of $(CeO_2)_{1-x}(BiO_{1.5})_x$. *Adv Mater* 1999;**11**: 146–9.
3. Chen XL, Eysel W. The stabilization of β-Bi_2O_3 by CeO_2. *J Solid State Chem* 1996;**127**:128–30.
4. Li Guangshe, li Liping, Feng Shouhua, wang Minqiang, Zhang Liangying, Yao Xi. Solid solubility and transport properties of nanocrystalline $(CeO_2)_{1-x}(BiO_{1,5})_x$ by hydrothermal conditions. *Chem Mater* 1999;**11**:1259–66.
5. Li Zhi-Cheng, Zhang Hong, Bergman Bill. Synthesis and characteration of nanostructured Bi_2O_3-doped cerium oxides fabricated by PVA polymerization process. *Ceram Int* 2007;**34**:1949–53.
6. Li Lindzhi, Yan Bing. CeO_2–Bi_2O_3 nanocomposite: two step synthesis, microstructure and photocatalytic activity. *J Non-Cryst Solids* 2009;**355**:776–9.
7. Bourja L, Bakiz B, Benlhachemi A, Ezahri M, Valmelette JC, Villain S, Gavarri JR. Structural and Raman Vibration Studies of CeO_2–Bi_2O_3 Oxide Systems. *Adv Mater Sci Eng* 2009:1–4.
8. Bošković S, Djurović D, Dohčević-Mitrović Z, Popović Z, Zinkevich M, Aldinger F. Self-propagating room temperature synthesis of nanopowders for solid oxide fuel cells (SOFC). *J Power Sources* 2005;**145**: 237–42.
9. Matovic B, Dohcevic-Mitrovic Z, Radovic M, Brankovic Z, Brankovic G, Boskovic S, Popovic ZV. Synthesis and characterization of ceria based nanometric powders. *J Power Sources* 2009;**193**:146–9.
10. Matovic B, Boskovic S, Logar M, Radovic M, Dohcevic-Mitrovic Z, Popovic ZV, Aldinger F. Synthesis and characterization of the nanometric Pr-doped ceria. *J Alloy Compd* 2010;**505**:235–8.
11. Prekajski M, Kremenović A, Babić B, Rosić M, Matovic B, Radosavljevic-Mihajlovic A, Radovic M. Room-temperature synthesis of nanometric α-Bi_2O_3. *Mater Lett* 2010;**64**:2247–50.
12. Rodriguez-Carvajal J, FullProf computer program, 1998, ftp://charybde.saclay.cea.fr/pub/divers/fullprof.98/windows/winfp98.zip.
13. Rodriguez-Carvajal. J. Recent advances in magnetic structure determination by neutron powder diffraction. *Physica B* 1993;**192**:55–69.
14. Rodríguez-Carvajal. J. Recent developments of the program FULLPROF, in Commission on Powder Diffraction (IUCr). *Newsletter* 2001;**26**:12–9, http://journals.iucr.org/iucr-top/comm/cpd/Newsletters/.
15. Balzar D, Audebrand N, Daymond MR, Fitch A, Hewat A, Langford JI, et al. *J Appl Crystall* 2004;**37**:911–24.
16. Barrett EP, Joyner LG, Halenda PP. The determination of pore volume and area distributions in porous substances. I Computations from nitrogen isotherms. *J Am Chem Soc* 1951;**73**:373–80.
17. Kaneko K, Ishii C, Ruike M, Kuwabara H. Origin of superhigh surface area and microcriystalline graphitic structures of activated carbons. *Carbon* 1992;**30**:1075–88.
18. Kruk M, Jaroniec M, Gadakaree KP. Nitrogen adsorption studies of novel synthetic active carbons. *J Colloid Interface Sci* 1997;**192**:250–6.
19. Kaneko K, Ishii C, Kanoh H, Hanzawa Y, Setoyama N, Suzuki T. Characterization of porous carbons with high resolution αs-analysis and low temperature magnetic susceptibility. *Adv Colloid Interface* 1998;**76-77**:295–320.
20. Kuemmerle EA, Heger G. The structures of C–$Ce_2O_{3+\delta}$, Ce_7O_{12}, and $Ce_{11}O_{20}$. *J Solid State Chem* 1999;**147**:485–500.
21. Hong SJ, Virkar AV. Lattice parameters and densities of rare earth oxide doped ceria electrolytes. *J Am Ceram Soc* 1995;**78**:433–9.
22. Yashima M, Ishizawa N, Yoshimura M. Application of an ion-packing model based on defect clusters to zirconia solid solutions. I Modeling and local structure of solid solutions. *J Am Ceram Soc* 1992;**75**:1541–9.
23. Ping L, Chen I, Hahn JE, Tien TY. X-ray absorption studies of ceria with trivalent dopants. *J Am Ceram Soc* 1991;**74**:958–67.
24. Hong SJ, Virkar AV. Lattice parameters and densities of rare-earth oxide doped ceria electrolytes. *J Am Ceram Soc* 1995;**78**:433–9.
25. Aškrabić S, Dohčević-Mitrović Z, Kremenović A, Lazarević N, Kahlenberg V, Popović ZV. Oxygen vacancy-induced microstructural changes of annealed CeO_{2-x} nanocrystals. *J Raman Spectrosc* 2011, accepted DOI 10.1002/jrs.2987.
26. Weber WH, Hass KC, McBride. JR. Raman study of CeO_2: second-order scattering, lattice dynamics, and particle-size effects. *Phys Rev B* 1993;**48**:17–85.
27. Kosacki I, Suzuki T, Anderson H, Colomban P. Raman scattering and lattice defects in nanocrystalline CeO_2 thin films. *Solid State Ionics* 2002;**149**:99–105.
28. Dohcevic-Mitrovic Z, Scepanovic MJ, Grujic-Brojcin MU, Popovic ZV, Boskovic S, Matovic B, Yinkevich MV, Aldinger F. The size and strain effects on the Raman spectra of $Ce_{1-x}Nd_xO_{2-\delta}$ ($0 \leq x \leq 0.25$) nanopowders. *Solid State Commun* 2006;**137**:387–90.
29. McBride JR, Hass KC, Poindexter BD, Weber WH. Raman and X-ray studies of $Ce_{1-x}RE_xO_{2-y}$, where RE = La Pr, Nd, Eu, Gd, and Tb. *J Appl Phys* 1994;**76**:2435–42.
30. Marabelli F, Wachter P. Covalent insulator CeO_2: optical reflectivity measurements. *Phys Rev B* 1987;**36**:1238–43.
31. Minervini L, Zacate MO, Grimes RW. Defect cluster formation in M_2O_3–doped CeO_2. *Solid State Ionics* 1999;**116**:339–49.